CHARACTERIZATION AND EVALUATION OF PROPERTIES OF NICOTINIUM P-TOLUENESULFONATE MONOHYDRATE (NPT) CRYSTAL

Abstract

Researchers have shown considerable enthusiasm for investigating novel organic materials that have the potential to show pharmaceutical and nonlinear optical (NLO) effects. Due to its vital function in effectively treating human illnesses, nicotinic acid, a key hydrophilic molecule included under the vitamin B complex, has garnered considerable attention in the pharmaceutical sector. During the current investigation, a good quality nicotinium p-toluenesulfonate monohydrate (NPT) single crystal was obtained with the help of SEST by taking equimolar amounts of nicotinic acid (NA) along with p-toluenesulfonic acid. Structural characterization of NPT was performed by powder x-ray diffraction (PXRD) and the structure was found well in accordance with the literature. The performance of NPT was assessed using various techniques. These investigations confirm its potential as a highly promising material with significant implications for a diverse range of applications in the field of nonlinear optical (NLO) applications.

Keywords: Crystal Growth, Dielectric, Nanoindentation.

Authors

Suminda
All India Jat Heroes Memorial College
Baba Mastnath University
Rohtak, Haryana, India.

Igor Bidkin
TEMA-NRD,
Department of Mechanical Engineering
Aveiro Institute of Nanotechnology (AIN)
University of Aveiro
Aveiro, Portugal.

Dr. Sonia
Baba Mastnath University
Rohtak, Haryana, India.

I. INTRODUCTION

Numerous investigations in the area of nonlinear optical (NLO) materials have been conducted since Townes et al. invented the laser in 1955. Within this field, when intense light is passed through an optical medium, new photon with varying photon energies are produced and along with this, coherence of the input light is also preserved. Two main nonlinear optical processes include second harmonic generation (SHG) and third harmonic generation (THG) which involve the generation of photons with doubled and tripled optical frequencies of the original light respectively [1,2]. Many of the crystal's properties are greatly influenced by its structure and symmetry.

Constant efforts are being made by researchers to find reliable and high-quality materials. They have successfully designed and synthesized various types of organic materials based on single crystal like materials containing D-Π-A interactions. In fact, the presence of a polar π-conjugated bond facilitates the formation of a push-pull conjugated structure with donor at one end and accepter at the other which facilitates the asymmetric charge distribution [3,4]. The kind of substituent (donor or acceptor), solvent polarity and temperature play a significant role in these conjugated intramolecular charge transfer (ICT) compounds [5-8]. Few researchers emphasize their research on the drug molecule Nicotinic acid (Niacin). It is a widely recognized hydrophilic pharmaceutical compound within the vitamin B complex group which is famous for its substantial therapeutic significance in addressing human diseases such as pellagra and shows many different pharmaceutical effects [9,10].

p-toluenesulfonic acid (tosylic acid) stands out as a formidable organic acid due to its remarkable nonlinear optical properties which arise from the considerable electron cloud delocalization within the sulfonate group of p-toluenesulfonate. Hence, its various derivatives are synthesized and analyzed for applications in multidisciplinary areas. Several previously reported crystals of p-toluenesulfonic acid show good NLO activities [11-20]. In this manuscript, we detail the preparation and growth of a hydrogen-bonded charge transfer (CT) complex of nicotinic acid (organic base) and p-toluenesulfonic acid (organic acid) thereby resulting in the formation of a non-centrosymmetric crystal lattice with commendable nonlinear optical characteristics. In the course of the proton transfer process, a proton takes place from the electron donating moiety of p-toluenesulfonic acid to the electron accepting group of nicotinic acid to form a zwitterion and also shows improved thermal and mechanical stability through hydrogen bonding interactions. Hence, it is projected as a forefront candidate for NLO applications. This article assesses various aspects of NPT single crystals in order to judge its applicability in device fabrication.

II. EXPERIMENTAL

The starting materials p-toluenesulfonic acid monohydrate and Nicotinic acid obtained from CDH Company are dissolved in distilled water in an equimolar ratio (1:1). The solution was subjected to continuous magnetic stirring for duration of 4 hours resulting in the formation of a homogeneous solution. This was subsequently filtered to eliminate impurities and allowed to undergo evaporative drying at ambient temperature. After a few days nucleation started and subsequently, got the transparent single crystals in five weeks. Fig.1 presents the photograph of the obtained crystal. The scheme for synthesis of nicotinium p-

toluenesulfonate monohydrate (NPT) is as follows:

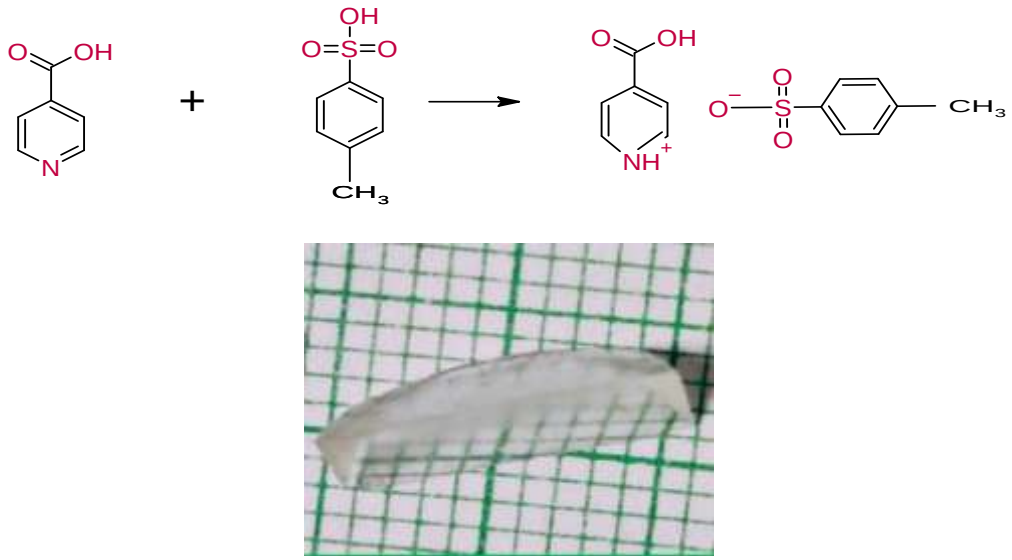

Figure 1: Picture Showing NPT Single Crystal

III. RESULTS AND DISCUSSION

1. **Powder X-ray Diffraction (PXRD)***:* PXRD has recently emerged as the most effective characterization method for structural investigation. The fundamental principle of X-ray diffraction theory lies in the phenomenon of constructive interference exhibited by monochromatic X-rays. The formed crystals were powdered and subjected to XRD having λ as 1.541836 Å to study the structure of the titled compound. The 2θ is varied from 10° to 50° with a step size of 0.02°. The depicted Fig. 2. Illustrates the recorded pattern obtained through PXRD. The experimental peaks were observed and exhibited excellent concurrence with the literature findings [21].

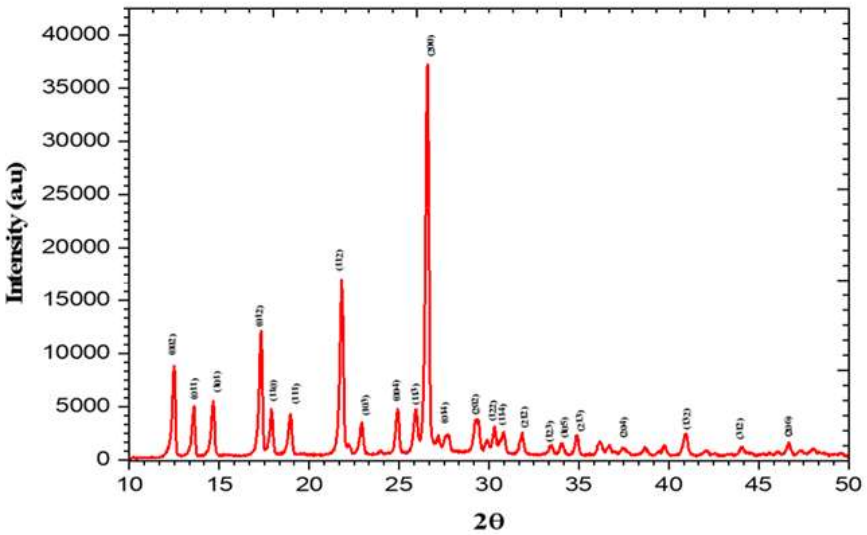

Figure 2: PXRD Plot for NPT Crystal

2. **Shock Damage Threshold:** In this contemporary era, the study of materials subjected to shock waves is becoming a popular area of study in the field of material science. It is a high-pressure phenomenon that is observed in events like volcanic eruptions, swiftly moving airplanes etc. It is one of the straight forward methods for studying the behaviour of materials under harsh conditions and for modifying their behaviour without changing the original crystal system. Shock waves can cause structural defects, phase shifts, orientation changes etc. in crystalline materials [22-23]. This study involves an investigation of the sample when exposed to shock waves up to Mach numbers 1.7 on NPT crystals using a shock tube. On increasing the shock, eventually, cracks start to appear. The sample was subjected to XRD to observe the effect of shock waves on the crystalline sample.

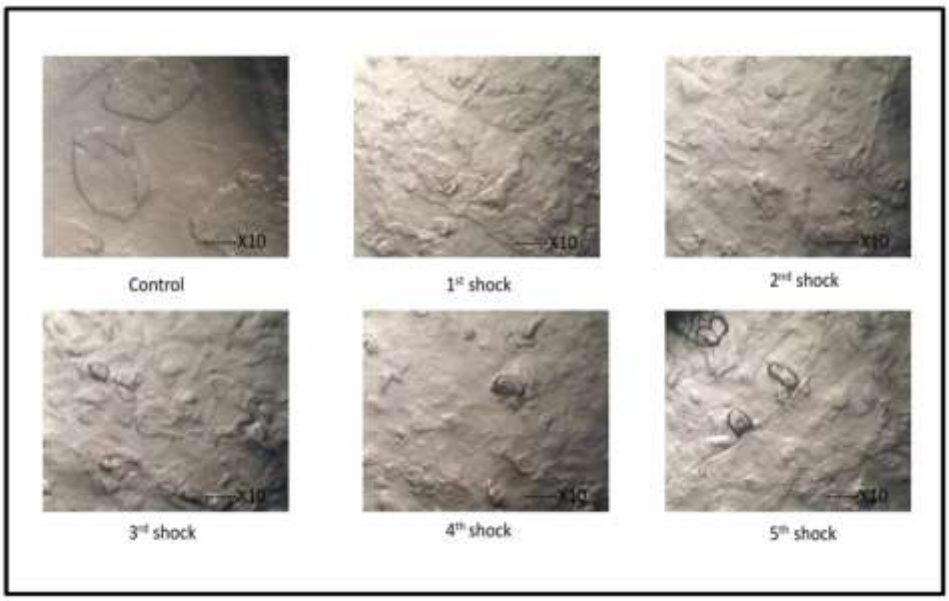

Figure 3: Optical Microscope Images of the Surface of the Crystal with 4X Magnification (A) Cleaned Surface with Solvent; (B) Surface Followed by 1st Shock; (C) Surface Followed By 2nd Shock; (D) Surface Followed by 3rd Shock; (E) Surface Followed by 4th Shock; (F) Surface Followed by 5th Shock For NPT Crystal

3. **Surface Morphology Studies:** Studies of surface morphology offer a fast and easy technique to identify surface defects, flatness or etch patterns. As a result, it makes a significant contribution to the materials' characterization under harsh conditions and an optical microscope is utilized to view the surface. Fig. 3 shows the optical micrographs (4×) for control and when subjected to shock waves of NPT crystals. The test crystal bent and showed defects that kept on increasing with progressive shocks and after 5^{th} shock, it cracked.

4. **Structural Properties:** It is possible to observe the changes occurring in structure-related characteristics of the crystals by examining the effect intense radiations or changing physical environments on them. In the present study, the sample was subjected to XRD having $\lambda = 1.5407$ Å for CuK α. The observed pattern for the sample before and after exposure to shock waves is shown in Fig. 4.

The obtained profiles provide conclusive evidence that NPT crystal does not undergo a structural phase change and no new crystalline peak creation or a peak disappearance has been seen. But a high degree of structural disorder is seen and peaks observed on successive shock wave conditions show an increase in full width half maximum (FWHM) on increasing shocks [24-26] which is shown in Fig. 5. All these may be caused due to increased misalignment in the atomic lattice plane, atomic displacements and modifications in the bonding scheme brought on by the influence of shock waves.

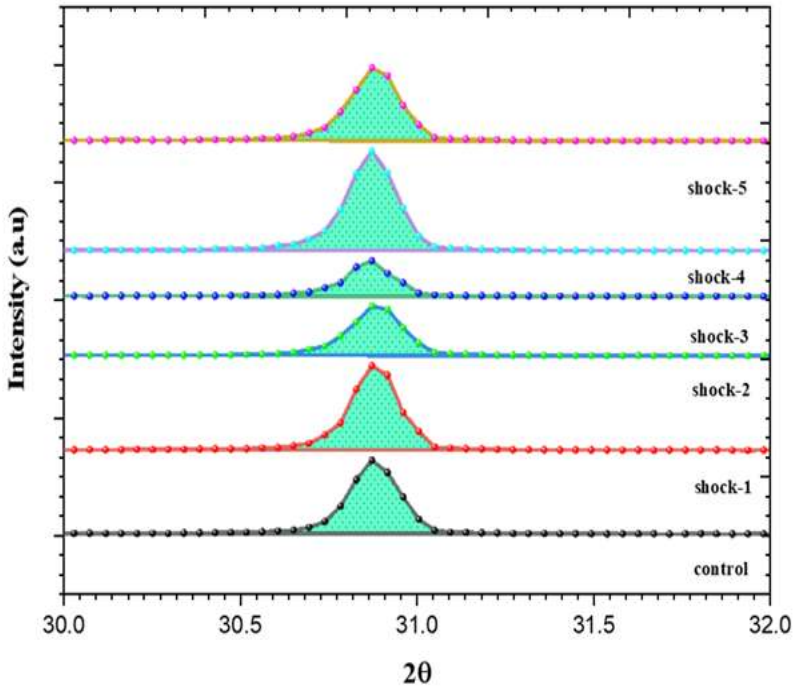

Figure 4: XRD Plot Before and After Exposure to Shock Wave for NPT Crystal

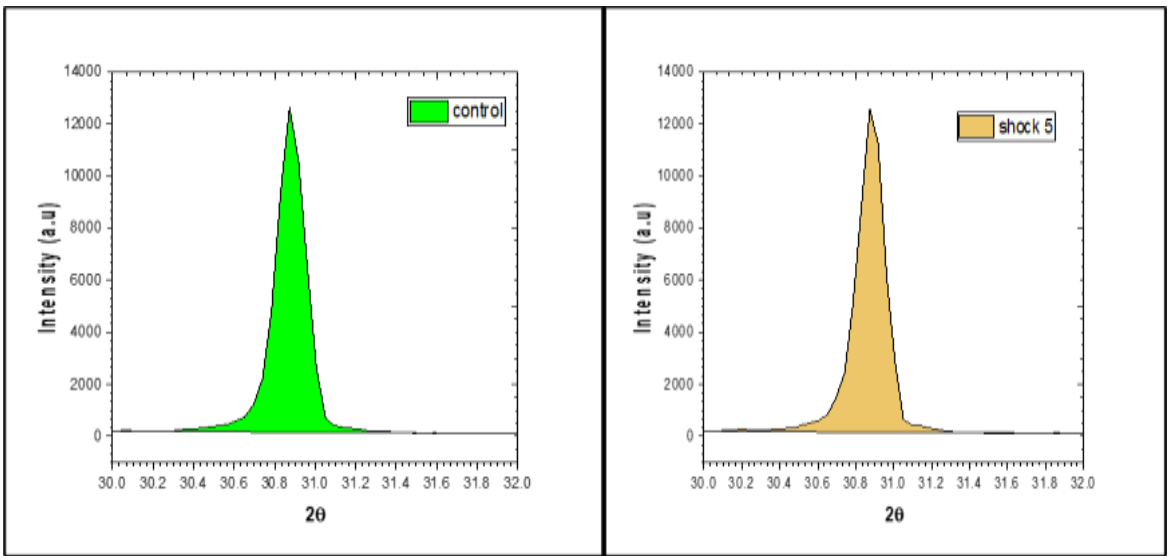

Figure 5: Comparision of XRD Pattern of Control and Post 5th Shock Wave for NPT Crystal

5. **Nanoindentation:** In recent times, engineers have shown increased interest in the nanoindentation technique, which involves evaluating the hardness-related parameters of single crystals. This technique allows for the correlation of measured properties with the underlying structural properties and intermolecular interactions. The findings obtained from these evaluations have numerous technical applications, including metallurgical industries, pharmaceuticals and molecular electronics [27]. The direction of the slip planes, twinning planes and cleavage planes on application indentation load determine the mechanical behaviour of single crystals. The nanoindentation technique uses the P–h responses for loading and unloading sequences for different loads in mN for measuring mechanical properties. This method can be used to investigate aspects such as anisotropy in molecular contacts, shear stability, evaluation of structural in homogeneities and stiffness of various bond types. In terms of studying a material's behaviour mechanically, its stiffness, strength and toughness are the fundamental properties. These characteristics provide indication of the material's resistance to cracking, as well as its ability to withstand elastic and plastic deformations. The most popular method for doing this is proposed by Oliver and Pharr which uses Berkovich tip nanoindenter. The schematic for the process of nanoindentation is presented in Fig. 6.

   In the current study, a well-polished single NPT crystal (plane (0-1 1)) was placed below a Berkovich tip and exposed to varying loads between 5 to 150 mN at an approach rate of 2000 nm/min approach rate. The indenter was well-calibrated from TTX-NHT, CSM Instruments. The P-h curves for different loads are presented in Fig. 7 Any surface changes caused by the indenter to the crystal, such as dents and fissures, can be seen using the AFM technique.

   The plastic (h_p) and elastic (h_e) deformations cause the total contact depth (h_t). These are then related to the hardness of the sample.In materials where no phase transition takes place the plasticity of the sample is attributed to the accumulation of material and the dislocation activity.

   As can be seen, the load-depth profiles are continuous and smooth during the curves with no noticeable pop-ins or pop-outs for maximum loads less than 20 mN. This shows that sample experiences elastic-plastic deformation at loads upto 20 mN without noticeable microcracking. But on increasing load over 20 mN, the noticeable pop-in are observed which keep on increasing up to 150 mN. This shows that the broad elastic-plastic deformation for a single crystal becomes substantial up to indentation stresses of 30 mN without cracking. The mechanical parameters for NPT crystal are tabulated in table 1.

   From the load-displacement curve it is evident that the crystal develops a micro-crack above 20 mN. Furthermore, the variation of modulus with load is exhibited in Fig. 8, which can be related to the ISE of the indenter and the intrinsic deformation. Also, h_c variation with f_{max} curve is shown in Fig. 9. Furthermore, load independent hardness (H_0) can be determined using the expression

$$H_0 = Ka_2, \text{ using } K = 1/24.5 \text{ for berkovich indenter} \quad (2)$$

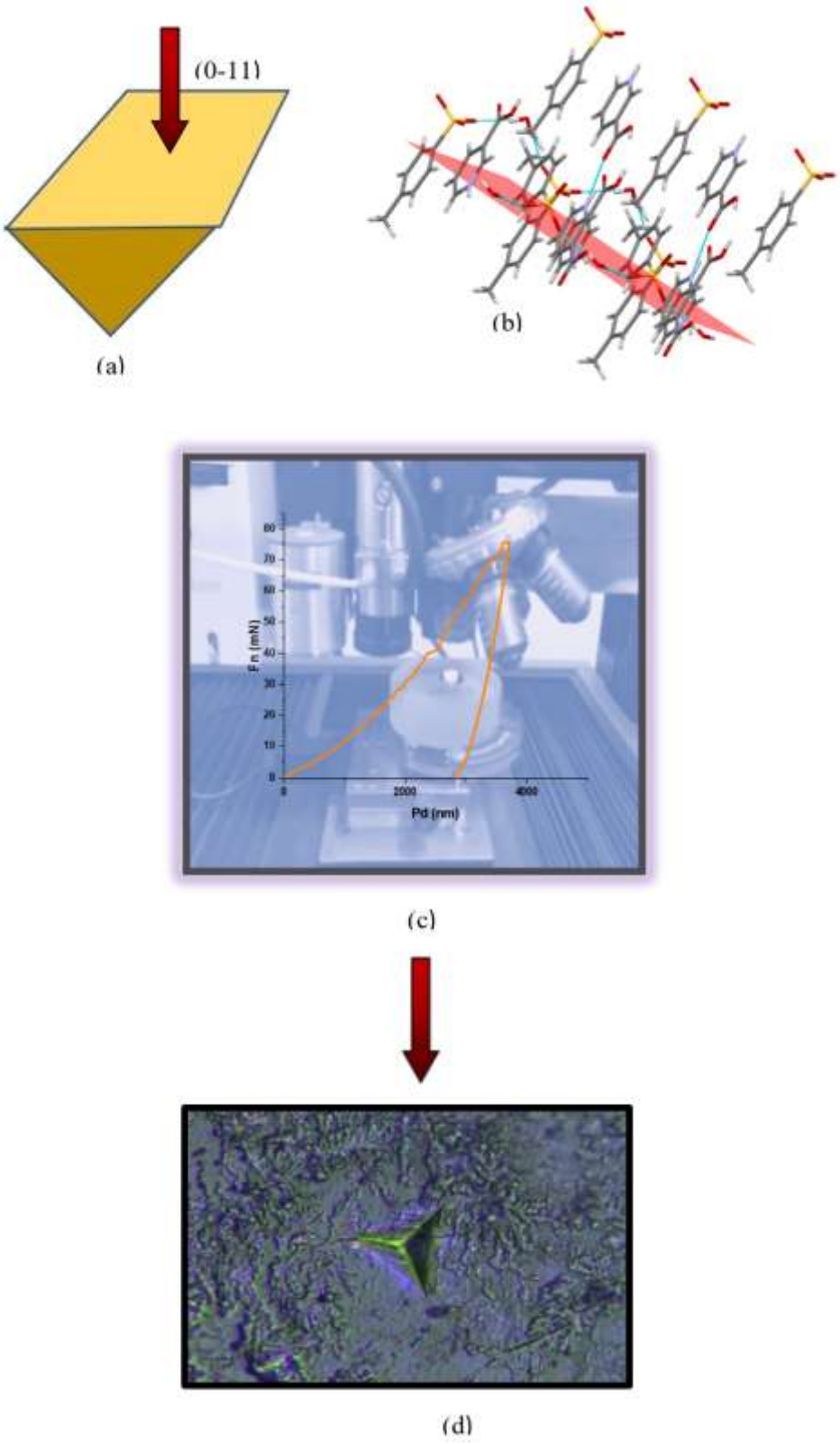

Figure 6: The Schematic for the Process of Nanoindentation for NPT Crystal (A) Crystal Morphology; (B) (0-11) Plane; (C) Load Displacement Graph; (D) Indentation Mark on the Surface of NPT Crystal

And a_2 obtained from the slope of the polynomial fitted graph for the given relation

$$F_{max} = a_0 + a_1 h_c + a_2 h_c^2 \quad (3)$$

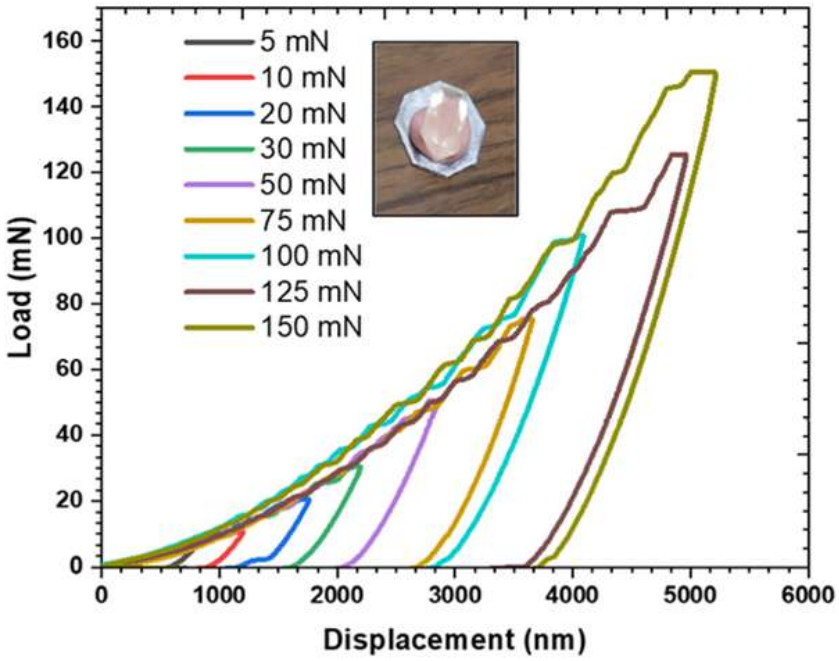

Figure 7: The P-h Curves for Different Loads for NPT Crystal. The Inset Shows NPT Crystal Used for Nanoindentation

Table 1: Mechanical Parameters Calculated From Loading and Unloading Curve of NPT Single Crystal

Fm (mN)	Hv	HIT (MPa)	EIT (GPa)	S (mN/nm)	h_c (nm)	m	h_m nm)	h_r (nm)	h_p (nm)	Poisson's ratio(σ)	Ap (nm^2)
5.54	79.108	854.19	12.363	0.0379	658.2951	1.36	771.17	624.314	595.723	0.30	6320415.2
10.59	77.979	842.01	11.688	0.0558	1071.713	1.39	1215.97	1022.47	845.062	0.30	1.34718E7
20.46	76.847	829.78	11.064	0.0711	1506.058	1.42	1708.53	1436.00	1176.65	0.30	2.45076E7
30.35	75.712	817.52	10.490	0.0828	1942.581	1.44	2233.60	1845.42	1571.90	0.30	3.78278E7
50.50	74.573	805.22	9.9674	0.0976	2506.347	1.46	2891.22	2381.06	2154.36	0.30	6.27329E7
75.48	73.430	792.88	9.4953	0.1161	3056.018	1.48	3542.69	2894.57	2558.61	0.30	8.93781E7
100.79	72.283	780.50	9.0739	0.1288	3661.352	1.49	4249.30	3465.57	3058.75	0.30	1.30079E8
125.44	71.133	768.08	8.7034	0.1420	4132.801	1.50	4799.79	3910.31	3460.77	0.30	1.65927E8
150.69	69.979	755.62	8.3837	0.1540	4520.837	1.50	5252.17	4277.20	3810.46	0.30	2.01888E8

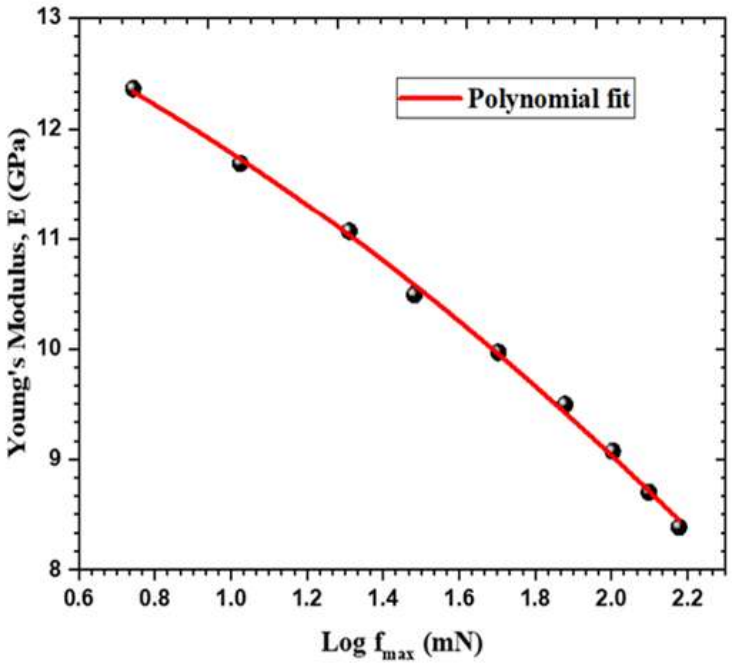

Figure 8: Variation of Young's Modulus with Log of Peak Load for NPT Crystal

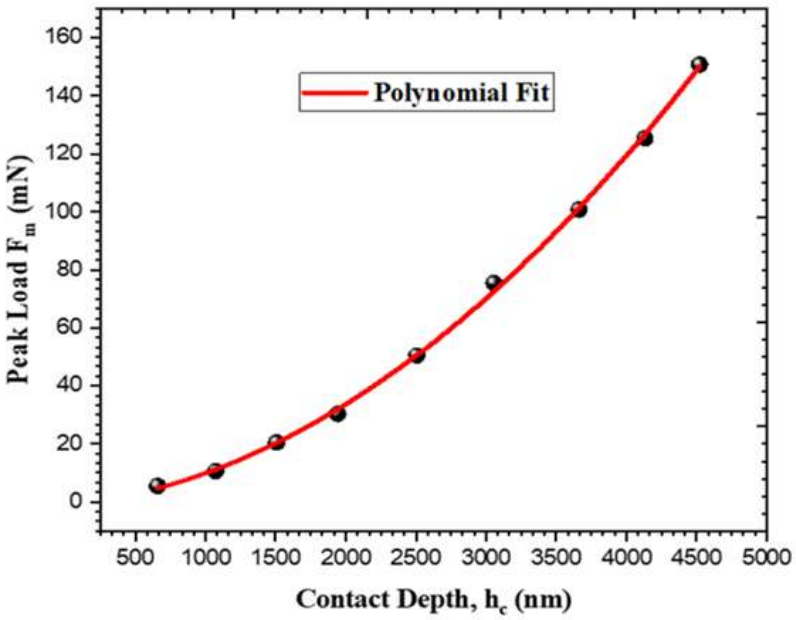

Figure 9: Variation of Hc with Peak Load for NPT Single Crystal

Also, Fig. 10 shows a linear relationship of stiffness S with h_c for NPT single crystal which are related as

$$S = a + bh_c \quad (4)$$

Here in 'a' represents a constant for the particular the indentation type while 'b' denotes the slope of the indentation created on the NPT single crystal. Experimental

findings revealed an intercept (a) of 0.024. Employing a linear regression analysis to elucidate young's modulus. The slope was found to be 2.892 x 10^{-5}mN nm^{-2}. So, the reduced young's modulus was estimated to be 28.92 GPA.

In addition to this, a stress-strain is plotted using the above data which is shown in Fig. 11. On fitting the polynomial curve, the coefficient a_0, a_1 and a_2 wereobtained. So, a_2 obtained is 6.347 x 10^{-6}mN nm^{-2}. Also, eqn. 2 gives the independent hardness as 0.258 GPa or 258 MPa. So, the titled compound offers a high resistance to deformation [28-30].

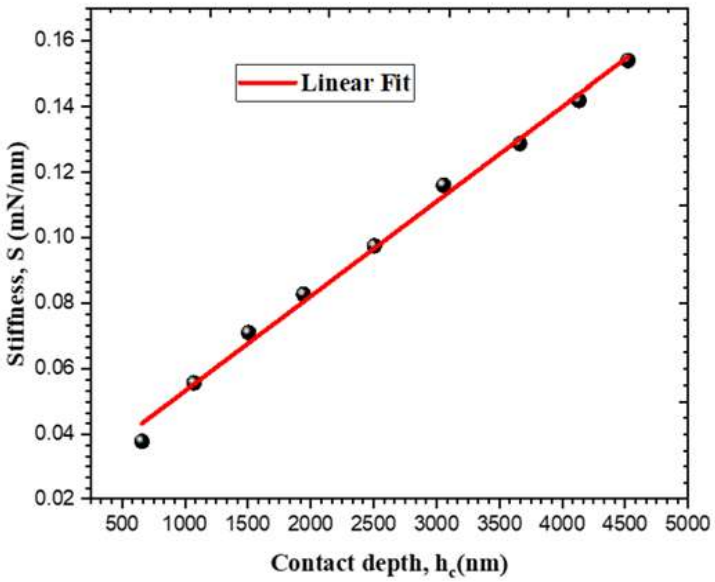

Figure 10: Variation of Stiffness with Peak Load for NPT Single Crystal

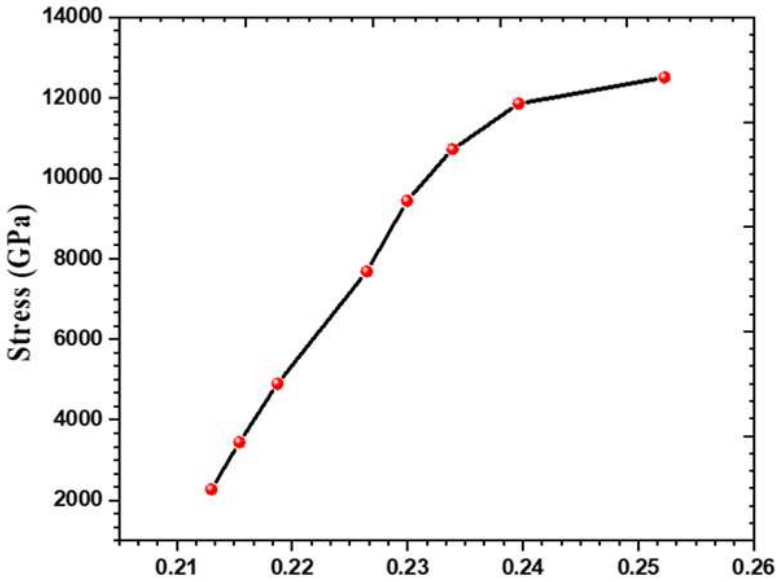

Figure 11: Stress-Strain Relation for NPT Single Crystal

6. **Impedance studies:** The dielectric analysis also provides the details on the location of grain boundaries, the amount of impurities and the presence of crystallographic defects [31-35]. In the present context, the dielectric parameters were studied for NPT crystal having thickness of 1mm by varying temperature from 30-60°C for 20 Hz–200 MHz frequency. At first, silver paste was put on both side of the crystal to make good electrical contacts and the potential difference of 1 V was kept during the experiment for the parallel plate capacitor. The dielectric constant (ϵ_r') can be obtained as

$$\epsilon_r' = C_p d/\varepsilon_0 A \quad (5)$$

C_p, A, d, ε_0 (8.85×10^{-12} F/m) are the capacitance, area, thickness and permittivity of the material respectively. It analyses the ability of materials to store electrical energy.

7. **Dependence of Dielectric Constant on Temperature:** ϵ_r' almost remains constant with the temperature at elevated frequencies. However, at low frequencies, ϵ_r'at 40°C slightly rises, as illustrated in Fig. 12, then returns to constant with rising temperature. This can be a result of structural modifications due to a change in contact strengths at intermediate temperatures. Water, being a polarized molecule, significantly impacts the crystal's dielectric properties. The molecular dipole orientation remains unchanged at lower temperatures due to intact bonds. As the temperature increases to 40°C, the strength between contacts weakens, allowing water molecules to realign themselves. This realignment is reflected with a rise in ϵ_r', particularly at smaller frequencies where polarization effects are more pronounced. ϵ_r' Eventually attains a stable value of 27 as the temperature continues to rise, indicating reduced polarization effects due to molecule dehydration.

8. **Frequency Dependent Variation of Dielectric Constant:** Its normal dielectric behaviour is illustrated in Fig. 13 in which the value of ϵ_r' decreases on increasing frequency which is influenced by the polarisation mechanisms. At low frequencies, the space charge polarization is the main polarisation mechanism which contribute to the value of ϵ_r'. Furthermore, the molecular dipole moments exhibit an enhanced responsiveness to the externally induced electric field [36].

With the increase in frequency, the contributions from different polarizations in the material start to decrease. The molecular dipole moments within the material are unable to respond quickly enough to the rapid changes in the applied electric field. Consequently, this results in a drop in capacitance and consequently, a drop in ϵ_r' value of the material. This constant value is attained at a higher frequency may be correlated to the material's structure and its polarization. The lower value of ϵ_r' signifies the good quality of the NPT crystal.

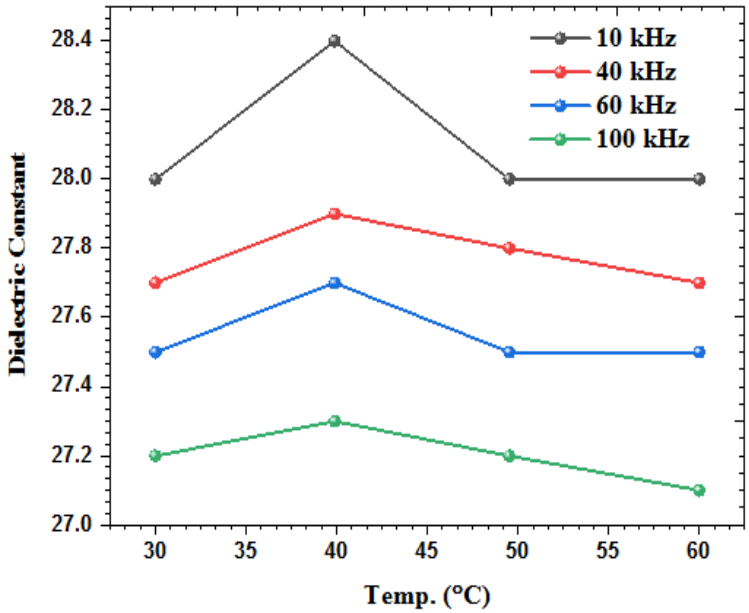

Figure 12: Dielectric Constant Variation with Temperature for NPT Single Crystal

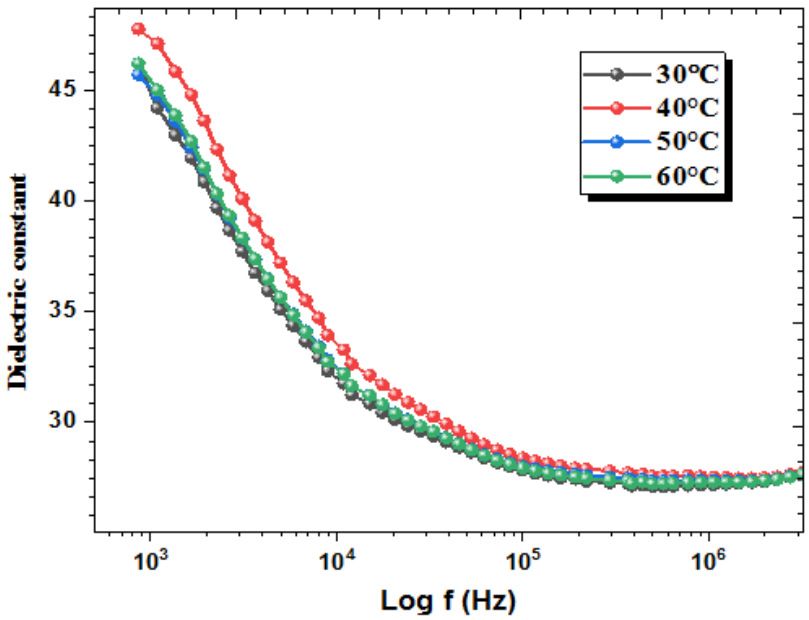

Figure 13: Plot for Frequency Dependent Variation of Dielectric Constant for NPT Single crystal

Furthermore, the slight variations observed in $\epsilon_r^{'}$ value with the temperature is attributed to the contribution of molecular permanent dipole moment in the process of polarization [37]. Its low dielectric constant value makes it a good photonic and electro-optic device material.

9. **Frequency Dependent Variation of Dielectric Loss:** The imaginary part of $\epsilon_r^{'}$ measures dielectric losses which can be calculated using the formula

$$\epsilon^{''} = \epsilon_r^{'} \times tan\,\delta \quad (6)$$

The relationship between dissipation (tan δ) and the frequency of the applied field is illustrated in Fig. 14 which shows a normal trend of decrease in dissipation with increased frequency. The good quality of the titled material is indicated by the low value of the dielectric loss. This loss factor, which is inversely proportional to its conductivity, represents the energy used to align the dipoles. As the frequency increases, the dipoles within the material gradually lose their ability to respond effectively to the rapidly changing electric fields. This leads to a decrease in their receptivity to such fields, resulting in a change in the value of dissipation with frequency [38]
8].

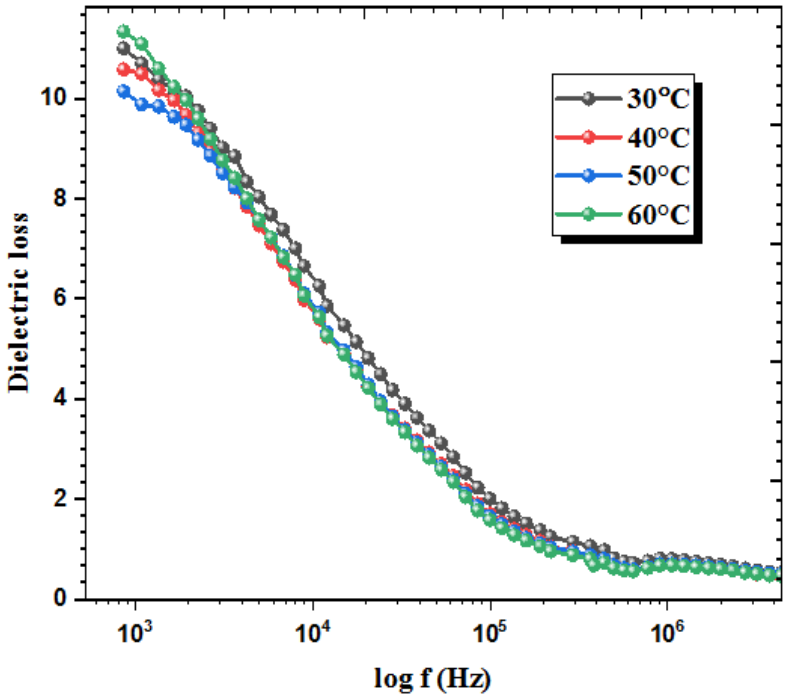

Figure 14: Impact of Frequency on Dielectric Loss Behaviour for NPT Single Crystal

10. **AC Conductivity (σ_{ac}) and Impedence:** The electrical conductivity is given as:

$$\sigma\,(\omega, T) = \sigma_{\mathrm{dc}}(T) + \sigma_{ac}(\omega, T) \quad (7)$$

where the σ_{dc} elucidates the temperature-dependent dc conductivity and σ_{ac} which is ac conductivity. Electrical conductivity is a defect-controlled process and studying this can provide important insights into the mobility, development and movement of lattice defects in hydrogen-bonded crystals [39]. The ac conductivity (σ_{ac}) of NPT crystals exhibits a pronounced frequency dependence of the applied ac field for varying temperatures shown in Fig. 15.

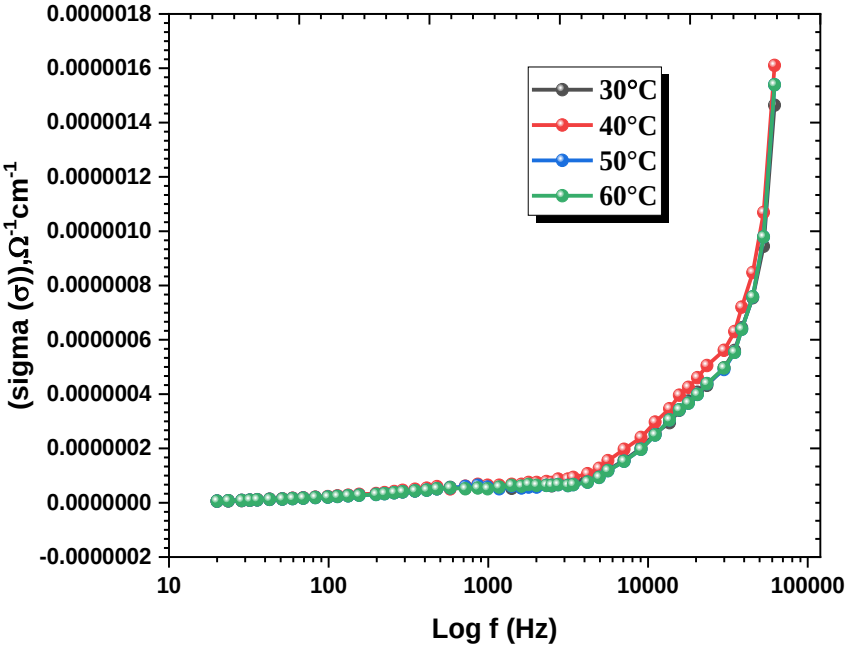

Figure 15: Variation of Sigma with Frequency for NPT Single Crystal

The ac conductivity is negligible at low frequency up to 100 kHz and then increases and attains maximum value. This can also be obtained from dielectric loss as

$$\sigma_{ac} = \omega \varepsilon_0 \epsilon_r' \tan \delta \quad (8)$$

Here tan δ represents the dielectric loss.

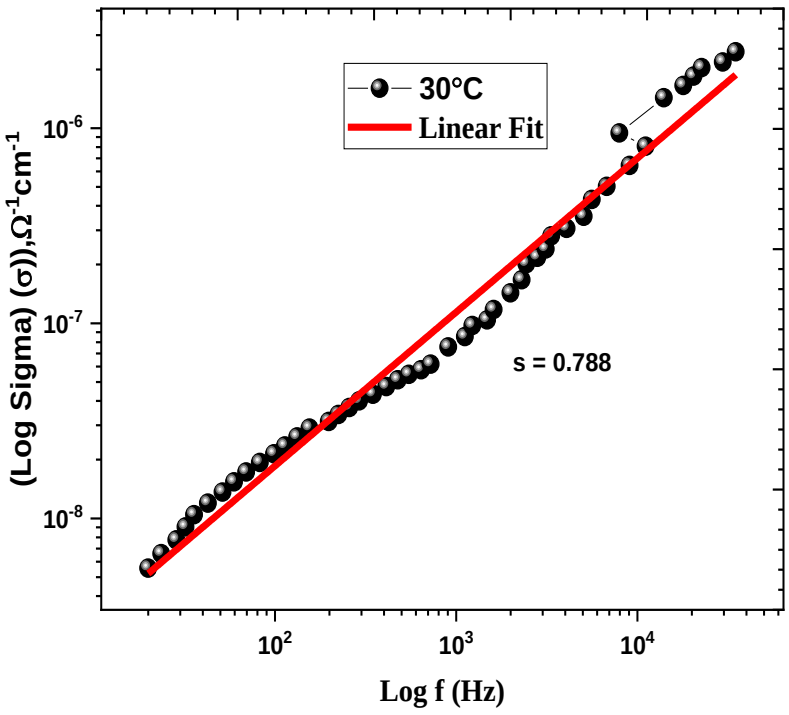

Figure 16: Frequency Dependent Variation of Log (Sigma) for NPT Single Crystal

The experimental results are justified by using different theories. One such theory is the polaron hopping model. According to this, the proton–phonon interaction occurs on the path of the proton and exhibits a strain field forming a quasi-particle like a polaron. The σ leads to greater values at longer frequencies at a given temperature. This trend supports the polaron hopping mechanism in NPT crystals. At higher frequencies, the polaron disperses and the protons travel forward, adding to the conductivity. Jonscher's universal power law relates σ_{ac} with ω as

$$\sigma(\omega) = A\omega^{s} \quad (9)$$

Where A is a constant, ω denotes the angular frequency and "s" is a dimensionless quantity which is almost independent of temperature and measures how much the mobile ions interact with the lattice [40-42]. The slope of the graph exhibited in Fig. 16 gives s = 0.788.

11. Impedance Analysis: It is a versatile approach to assess different electrical parameters of various ion conducting solids. It gives vital information about the bulk and surface properties of these materials. Fig. 17 demonstrates the frequency-dependent variation of impedance (Z') across varying temperatures for NPT crystal.

The graph shows that Z' has inverse relation with frequency and temperature. For larger values of frequencies, it shows a constant value which can potentially be attributed to the release of space charge.

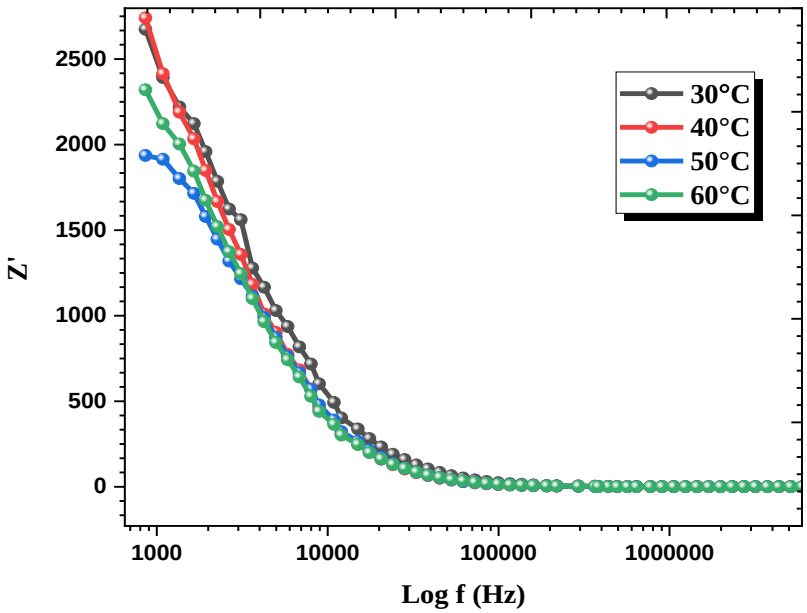

Figure 17: Variation of Impedance with Frequency for NPT Single Crystal

IV. CONCLUSIONS

The transparent organic NPT single crystal was grown and subjected to various characterizations in order to access its potential applications. PXRD analysis of the crystal unfolds the information about its space group and lattice parameters which were found to be same as in literature. Nanoindentation results manifested the better endurance and mechanical strength of the title compound. The Shock Damage Threshold for NPT on impulsion of shock waves was determined. This investigation highlighted the crystal's resilience under harsh conditions and also provided insights into structural defects along with changes induced by the shock waves. The study of structural properties through XRD before and after exposure to shock waves further reinforced the material's stability, indicating no structural phase changes. However, the increase in full width half maximum (FWHM) suggested a high degree of structural disorder, which could be attributed to modifications in the bonds caused by the shock waves. Its various dielectric parameters were also investigated. The dielectric analysis revealed important information about grain boundaries, impurities, and crystallographic defects, while the frequency-dependent behaviour of dielectric constants and losses supported the material's quality and potential for photonic and electro-optic applications. These findings prove it to be a promising material for NLO applications.

REFERENCES

[1] Sonia et al., “An efficient piezoelectric single-crystal l-argininium phosphite: structural, Hirshfeld, electrical and mechanical analyses for NLO applications,” Appl. Phys. A, vol. 125, no. 5, pp. 363–377, Apr. 2019, doi: 10.1007/s00339-019-2642-5.

[2] N. Vijayan et al., “Growth and Characterization of Nonlinear Optical Amino Acid Single Crystal: l - Alanine,” Crystal Growth & Design, vol. 6, no. 11, pp. 2441–2445, Nov. 2006, doi: 10.1021/cg049594y.

[3] M. Kumari, N. Vijayan, D. Nayak, M. Kumar, G. Gupta, and R. P. Pant, “Assessment of optical, mechanical and nonlinear properties of potassium acid phthalate single crystal: a potential candidate for optoelectronic applications,” Mater. Res. Express, vol. 7, no. 1, pp. 015705–015717, Jan. 2020, doi: 10.1088/2053-1591/ab619e.

[4] P. Era, Ro. Mu. Jauhar, G. Vinitha, and P. Murugakoothan, “Synthesis, growth, structural modeling and physio-chemical properties of a charge transfer molecule: Guanidinium tosylate,” Optics & Laser Technology, vol. 101, pp. 127–137, May 2018, doi: 10.1016/j.optlastec.2017.11.005.

[5] G. Peramaiyan, R. M. Kumar, and G. Bhagavannarayana, “Crystal growth, structural, optical and dielectric studies of ammonium p-toluenesulfonate,” Journal of Crystal Growth, vol. 408, pp. 14–18, Dec. 2014, doi: 10.1016/j.jcrysgro.2014.09.011.

[6] H. Anizaim, S. Arshad, M. F. Zaini, M. Abdullah, D. A. Zainuri, and I. A. Razak, “Third order nonlinear optical properties of selected fluorinated chalcone derivatives,” Optical Materials, vol. 98, p. 109406, Dec. 2019, doi: 10.1016/j.optmat.2019.109406.

[7] K. Thukral et al., “In-depth behavioral study of l-Prolinium Trichloroacetate single crystal: An efficient candidate for NLO applications,” Arabian Journal of Chemistry, vol. 12, no. 8, pp. 4887–4896, Dec. 2019, doi: 10.1016/j.arabjc.2016.09.011.

[8] E. W. Meijer, E. E. Havinga, and G. L. J. A. Rikken, “Second-harmonic generation in centrosymmetric crystals of chiral molecules,” Phys. Rev. Lett., vol. 65, no. 1, pp. 37–39, Jul. 1990, doi: 10.1103/PhysRevLett.65.37.

[9] Datta and S. K. Pati, “Charge-Transfer Induced Large Nonlinear Optical Properties of Small Al Clusters: Al 4 M 4 (M = Li, Na, and K),” J. Phys. Chem. A, vol. 108, no. 44, pp. 9527–9530, Nov. 2004, doi: 10.1021/jp047204c.

[10] S. R. Marder, J. W. Perry, and C. P. Yakymyshyn, “Organic Salts with Large Second-Order Optical Nonlinearities,” Chem. Mater., vol. 6, no. 8, pp. 1137–1147, Aug. 1994, doi: 10.1021/cm00044a012.

[11] M. Suresh, S. A. Bahadur, and S. Athimoolam, “Crystal Growth and Characterization of a New NLO Material: p-Toluidine p-Toluenesulfonate,” Indian Journal of Materials Science, vol. 2013, pp. 1–4, Dec. 2013, doi: 10.1155/2013/680256.

[12] M. Suresh, S. Asath Bahadur, and S. Athimoolam, "Synthesis, growth and characterization of a new hydrogen bonded organic tosylate crystal: l-alaninium p-toluenesulfonate for second order nonlinear optical applications," J Mater Sci: Mater Electron, vol. 27, no. 5, pp. 4578–4589, May 2016, doi: 10.1007/s10854-016-4334-7.

[13] P. Era, Ro. Mu. Jauhar, P. Vivek, and P. Murugakoothan, "Investigation on the optical, electronic, mechanical and thermal parameters of guanidinium p-toluenesulfonate single crystal for opto-electronic applications," Materials Chemistry and Physics, vol. 257, p. 123647, Jan. 2021, doi: 10.1016/j.matchemphys.2020.123647.

[14] G. Shanmugam and S. Brahadeeswaran, "Spectroscopic, thermal and mechanical studies on 4-methylanilinium p-toluenesulfonate – a new organic NLO single crystal," Spectrochimica Acta Part A: Molecular and Biomolecular Spectroscopy, vol. 95, pp. 177–183, Sep. 2012, doi: 10.1016/j.saa.2012.04.100.

[15] G. Sivaraj, N. Jayamani, and V. Siva, "Synthesis, structural, spectroscopic, mechanical, linear and nonlinear optical studies on 4-dimethylaminopyridinium p-toluenesulfonate: A comparative theoretical and experimental investigation," Journal of Molecular Structure, vol. 1240, p. 130530, Sep. 2021, doi: 10.1016/j.molstruc.2021.130530.

[16] G. Peramaiyan, R. M. Kumar, and G. Bhagavannarayana, "Crystal growth, structural, optical and dielectric studies of ammonium p-toluenesulfonate," Journal of Crystal Growth, vol. 408, pp. 14–18, Dec. 2014, doi: 10.1016/j.jcrysgro.2014.09.011.

[17] M. Suresh, S. A. Bahadur, and S. Athimoolam, "Investigations on spectroscopic, optical, thermal and dielectric properties of a new NLO material: l-Histidinium p-toluenesulfonate [LHPT]," Optik, vol. 126, no. 24, pp. 5452–5455, Dec. 2015, doi: 10.1016/j.ijleo.2015.09.037.

[18] V. Thayanithi and P. P. Kumar, "Growth, optical, mechanical and thermal behavior of unidirectionally grown L-Glutaminium p-Toluenesulfonate crystal," Mater. Res. Express, vol. 6, no. 4, p. 046207, Jan. 2019, doi: 10.1088/2053-1591/aafd43.

[19] M. Suresh, S. Asath Bahadur, and S. Athimoolam, "Structural and solid state properties of l-leucinium p-toluenesulfonate monohydrate: an amino acid tosylate NLO crystal," J Mater Sci: Mater Electron, vol. 28, no. 1, pp. 661–672, Jan. 2017, doi: 10.1007/s10854-016-5572-4.

[20] P. Prabu, R. Aarthi, and C. Ramachandra Raja, "Growth and characterization studies on L-threoninium p-toluenesulfonate monohydrate crystal," Opt Quant Electron, vol. 51, no. 5, p. 143, May 2019, doi: 10.1007/s11082-019-1862-4.

[21] V. Thayanithi, B. Gunasekaran, and P. P. Kumar, "Growth, optical, dielectrical, thermal and mechanical behavior of organic nonlinear optical Nicotinium p-toluenesulfonate monohydrate single crystal," Optik, vol. 194, p. 163048, Oct. 2019, doi: 10.1016/j.ijleo.2019.163048.

[22] G. Jagadeesh, "Fascinating world of shock waves," Reson, vol. 13, no. 8, pp. 752–767, Aug. 2008, doi: 10.1007/s12045-008-0082-1.

[23] S. Aswathappa et al., "Shock wave induced defect engineering on structural and optical properties of pure and dye doped potassium dihydrogen phosphate crystals," Zeitschrift für Kristallographie - Crystalline Materials, vol. 235, no. 6–7, pp. 193–202, Jul. 2020, doi: 10.1515/zkri-2020-0017.

[24] Sivakumar, M. Manivannan, S. Sahaya Jude Dhas, J. Kalyana Sundar, M. Jose, and S. A. M. B. Dhas, "Tailoring the dielectric properties of KDP crystals by shock waves for microelectronic and optoelectronic applications," Mater. Res. Express, vol. 6, no. 8, p. 086303, May 2019, doi: 10.1088/2053-1591/ab1c96.

[25] Sivakumar, S. Reena Devi, J. Thirupathy, R. Mohan Kumar, and S. A. Martin Britto Dhas, "Effect of Shock Waves on Structural, Thermophysical and Dielectric Properties of Glycine Phosphate (GPI) Crystal," Journal of Elec Materi, vol. 48, no. 11, pp. 7216–7225, Nov. 2019, doi: 10.1007/s11664-019-07510-1.

[26] Gorel et al., "Shock Damage Analysis in Serial Femtosecond Crystallography Data Collected at MHz X-ray Free-Electron Lasers," Crystals, vol. 10, no. 12, p. 1145, Dec. 2020, doi: 10.3390/cryst10121145.

[27] G. Guillonneau, G. Kermouche, S. Bec, and J.-L. Loubet, "Determination of mechanical properties by nanoindentation independently of indentation depth measurement," J. Mater. Res., vol. 27, no. 19, pp. 2551–2560, Oct. 2012, doi: 10.1557/jmr.2012.261.

[28] Z. Ma, R. P. Gamage, and C. Zhang, "Mechanical properties of α-quartz using nanoindentation tests and molecular dynamics simulations," International Journal of Rock Mechanics and Mining Sciences, vol. 147, p. 104878, Nov. 2021, doi: 10.1016/j.ijrmms.2021.104878.

[29] S. Sonia et al., "Assessment of the imperative features of an l -arginine 4-nitrophenolate 4-nitrophenol dihydrate single crystal for non linear optical applications," Mater. Chem. Front., vol. 1, no. 6, pp. 1107–1117, 2017, doi: 10.1039/C6QM00217J.

[30] K. Thukral et al., "Growth, structural and mechanical analysis of a single crystal of L-prolinium tartrate: a promising material for nonlinear optical applications," CrystEngComm, vol. 16, no. 39, pp. 9245–9254, Sep. 2014, doi: 10.1039/C4CE01232A.
[31] J. B. Charles and F. D. Gnanam, "Dielectric studies on sodium fluoroantimonate single crystals," Cryst. Res. Technol., vol. 29, no. 5, pp. 707–712, 1994, doi: 10.1002/crat.2170290525.
[32] D. Nayak et al., "Bulk growth of Iminodiacetic acid single crystal and its characterization for nonlinear optical applications," Bulletin of Materials Science, vol. 44, p. 55, Mar. 2021, doi: 10.1007/s12034-020-02338-6S.
[33] G. Peramaiyan, R. M. Kumar, and G. Bhagavannarayana, "Crystal growth, structural, optical and dielectric studies of ammonium p-toluenesulfonate," Journal of Crystal Growth, vol. 408, pp. 14–18, Dec. 2014, doi: 10.1016/j.jcrysgro.2014.09.011.
[34] Hooda, S. Sanghi, A. Agarwal, and R. Dahiya, "Crystal structure refinement, dielectric and magnetic properties of Ca/Pb substituted SrFe 12 O 19 hexaferrites," Journal of Magnetism and Magnetic Materials, vol. 387, pp. 46–52, Aug. 2015, doi: 10.1016/j.jmmm.2015.03.078.
[35] S. A. M. B. Dhas, G. Bhagavannarayana, and S. Natarajan, "Growth, HRXRD, Microhardness and Dielectric Studies on the NLO Material L-Alaninium Maleate," TOCRYJ, vol. 1, no. 1, pp. 42–45, Oct. 2008, doi: 10.2174/1874846500801010042.
[36] H. Bouaamlat et al., "Dielectric Properties, AC Conductivity, and Electric Modulus Analysis of Bulk Ethylcarbazole-Terphenyl," Advances in Materials Science and Engineering, vol. 2020, pp. 1–8, Jan. 2020, doi: 10.1155/2020/8689150.
[37] S. Suresh, "The Growth and the Optical, Mechanical, Dielectric and Photoconductivity Properties of a New Nonlinear Optical Crystal—L-Phenylalanine-4-nitrophenol NLO Single Crystal," JCPT, vol. 03, no. 03, pp. 87–91, 2013, doi: 10.4236/jcpt.2013.33014.
[38] M. Sindhu, N. Ahlawat, S. Sanghi, A. Agarwal, R. Dahiya, and N. Ahlawat, "Rietveld refinement and impedance spectroscopy of calcium titanate," Current Applied Physics, vol. 12, no. 6, pp. 1429–1435, Nov. 2012, doi: 10.1016/j.cap.2012.03.034.
[39] S. F. Chérif, A. Chérif, W. Dridi, and M. F. Zid, "Ac conductivity, electric modulus analysis, dielectric behavior and Bond Valence Sum analysis of Na3Nb4As3O19 compound," Arabian Journal of Chemistry, vol. 13, no. 6, pp. 5627–5638, Jun. 2020, doi: 10.1016/j.arabjc.2020.04.003.
[40] M. D. Shah and B. Want, "Dielectric and conducting behavior of gadolinium–terbium fumarate heptahydrate crystals," J. Adv. Dielect., vol. 05, no. 03, p. 1550020, Sep. 2015, doi: 10.1142/S2010135X15500204.
[41] S. P. Rathee and D. S. Ahlawat, "Spectroscopic and thermo- electrical investigation of single crystals of l-Ornithine monohydrochloride grown by SEST," Optik, vol. 136, pp. 249–258, May 2017, doi: 10.1016/j.ijleo.2017.02.045.
[42] Saranraj, J. Thirupathy, S. S. J. Dhas, M. Jose, G. Vinitha, and S. A. M. B. Dhas, "Growth and characterization of unidirectional benzil single crystal for photonic applications," Appl. Phys. B, vol. 124, no. 6, p. 97, Jun. 2018, doi: 10.1007/s00340-018-6971-4.

